JOURNAL OF Materials CHEMISTRY

Carbon nanotube films obtained by thermal chemical vapour deposition

Oleg A. Nerushev, Martin Sveningsson, Lena K. L. Falk and Frank Rohmund*

School of Physics and Engineering Physics, Gothenburg University and Chalmers University of Technology, S-412 96 Gothenburg, Sweden. E-mail: frankr@fy.chalmers.se; Fax: +46 31 772 3496; Tel: +46 31 772 3432

Received 6th December 2000, Accepted 2nd February 2001
First published as an Advance Article on the web 6th March 2001

Films of carbon nanotubes are interesting for technical applications such as cold cathodes in field emission devices. We discuss experiments in which nanotube films are grown by a simple thermal chemical vapour deposition method from hydrocarbon molecules, employing the catalytic activity of deposited iron particles. Using an *in situ* catalyst preparation method starting from gaseous $Fe(CO)_5$, films of vertically aligned and non-aligned multi-wall carbon nanotubes can be synthesised. Nanotube film growth is discussed as a function of the growth conditions. Steps towards the formation of horizontally aligned nanotube films and nanotube patterns are presented. Field emission measurements demonstrate the high electron emission efficiency of the as-grown films.

1. Introduction

Carbon nanotubes are considered to be among the technologically most promising nano-scale materials due to their extraordinary electronic and mechanical properties[1] with the potential to find applications in various fields of science and engineering.[2] As individual objects, they can serve as active electronic elements in nanometre-sized electric circuits[3] or tips in scanning probe microscopy.[4] New kinds of composite materials containing carbon nanotubes as reinforcing agent could provide extremely strong but also lightweight construction materials for advanced applications.

Progress towards industry-scale applications of carbon nanotubes is hampered by the difficulty of producing sufficient amounts of carbon nanotube material. High quality material of very limited quantity can be produced by arc discharge and laser vapourisation of graphite (see ref. 5 for a recent review on production techniques). More promising for large-scale synthesis of carbon nanotubes are methods based on chemical vapour deposition (CVD) of carbon from molecular precursors, assisted by the catalytic activity of small transition metal particles.[6] Thermal catalytic CVD can be employed to obtain single-wall carbon nanotubes (SWNT) on supported metal particles[7–18] and in the gas phase[19–21] as well as multi-wall carbon nanotubes (MWNT) on deposited catalyst particles[22–40] and in the gas phase[41,42] from hydrocarbon and carbon monoxide precursor molecules. MWNT can also be obtained by pyrolysis of organometallic compounds,[43,44] catalytic disproportionation of fullerenes[45,46] as well as a variety of plasma assisted catalytic CVD processes[47–58] from hydrocarbons. Similar CVD methods can be utilised for the growth of BN,[59] B_xC_{1-x},[60] C_xN_{1-x}[61–65] and $B_xC_yN_z$[66–68] MWNT.

Non-gas phase CVD techniques allow, besides production of bulk amounts of nanotubes, synthesis of nanotube films directly on substrates. The nanotube structures and film morphologies depend on the growth process used. Among the most interesting ones are films of vertically aligned carbon nanotubes which can be obtained by both thermal[28,34–36,38,39,44] and plasma assisted[50–58] CVD methods. The excellent field emission properties of carbon nanotubes[69] suggest the use of carbon nanotube films as cathodes in flat panel displays,[70] field emission lamps[71] and related technologies. It is very likely that the first commercialisation of carbon nanotubes will be found here.

In this contribution we will discuss the formation of carbon nanotube films by thermal CVD from hydrocarbon molecules on iron catalyst particles. We will show that different film morphologies can be achieved. The nanotube film growth process will be discussed as well as the properties of the nanotubes as a function of the growth conditions.

2. Experimental

Nanotube growth by thermal CVD is performed in a horizontal tube furnace as shown in Fig. 1. The inner diameter of the process tube is 20 mm, the heated length 20 cm. This apparatus allows the iron-catalysed production of both SWNT[20] and MWNT,[72] depending on the carbon feedstock gas. In this paper we will limit the discussion to the growth of MWNT on supported iron particles from hydrocarbon molecules. Hydrocarbon molecules (C_2H_2 or CH_4) are

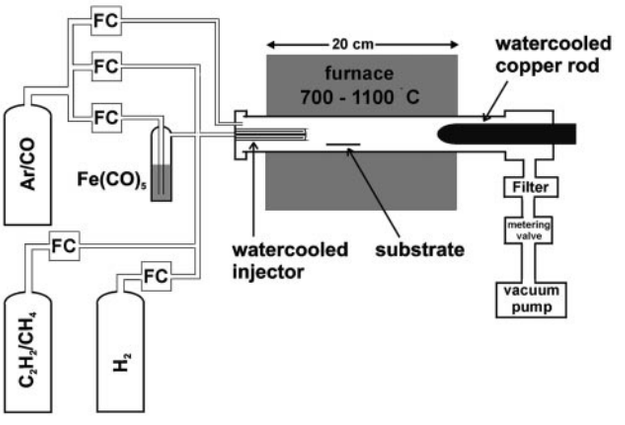

Fig. 1 The CVD production apparatus. The furnace holds a quartz tube of 20 mm inner and 25 mm outer diameter with a heated length of 200 mm. Gases are taken from high pressure gas tanks without further purification and fed into the hot zone of the furnace through a water-cooled injector. The total flow of the buffer/carrier gas (Ar or CO) is 600 sccm. A moderate carrier flow of 100 sccm around the cold injector prohibits a standing gas volume in this region. Liquid $Fe(CO)_5$ is placed in a glass bubbler and protected from light to inhibit photolysis. A fraction of the carrier flow transports the carbonyl vapour into the furnace. A water-cooled copper rod cools the exhaust gas and serves as a condenser for gas phase reaction products.

 DOI: 10.1039/b009775f

This journal is © The Royal Society of Chemistry 2001

introduced into the system *via* rotameter flow meters, along with Ar or CO as buffer and carrier gas and H_2 as reducing agent. Dilution of the hydrocarbon gases with an excess of argon (or CO) is necessary in order to avoid formation of unwanted pyrolysis products of the hydrocarbons. Dilution factors vary between 20 and 70. The process pressure is one atmosphere.

The iron catalyst is prepared by two different procedures. In the first, iron is delivered into the tube furnace in the form of gaseous $Fe(CO)_5$. For this purpose, a small fraction of the carrier gas flow is fed through a bubbler which is filled with the liquid carbonyl and held at 0 °C. The vapour pressure of the carbonyl at this temperature is 9.3 mbar. Thermal decomposition of these molecules at elevated temperatures *via* loss of CO units leads to the formation of atomic iron which deposits on the surfaces in the hot zone of the furnace and forms an iron film. To inhibit deposition of the iron atoms in the transition zone in front of the hot zone of the furnace it is, together with the remaining gases, introduced into the furnace through a water-cooled injector which protrudes a few centimetres into the hot zone. Nanotube growth can be achieved simultaneously with the introduction of the iron pentacarbonyl, *i.e.* during co-deposition of iron and carbon, at temperatures which are sufficiently high for nanotube growth. Depending on the carbon feedstock, the nanotube growth temperature varies between 750 °C (for acetylene) and 1100 °C (for methane). Iron films can also be prepared at a lower temperature, typically 200 °C, in the absence of hydrocarbons, hence without the formation of carbon nanotubes, while the nanotubes are grown in a second step at the higher nanotube growth temperature (see above) without providing additional $Fe(CO)_5$.

Deposited iron catalyst particles were also obtained by substrate impregnation with 50 mM $Fe(NO_3)_3 \cdot 9H_2O$ solutions in ethanol. The nitrate solution is deposited on the substrate, after a given period of time the solution is removed, followed by washing with de-ionised water and blowing off the remaining liquid with an air gun. The iron nitrate covered substrates are then transferred into the CVD furnace. Alternatively, a nitrate covered substrate is directly transfered into the CVD furnace and the ethanol is removed by pumping out the furnace with a vacuum pump. In the latter case a visible coating on the substrate is achieved, while after application of the former method the substrates appear visibly blank. Upon heating of the substrates in a reducing hydrogen–argon atmosphere, iron nitrate will first decompose with formation of iron ions which are subsequently reduced at a higher temperature by the hydrogen, thus forming elemental iron particles which can serve as catalysts for nanotube growth.

Polished Si(100) wafer pieces (10×30 mm surface area) were used as substrates. Before processing, they were cleaned in acetone in an ultrasound bath for a few minutes. Deposition of catalyst and nanotube films was carried out on the natural oxide surface of the Si wafer.

Field emission of electrons from carbon nanotube films was measured using a hemispherical anode with a radius R of 2 mm at a distance Z of 100 μm from the as-produced nanotube film. A negative voltage V is applied to the nanotube film, the field emission current I is measured with a picoammeter. For the determination of the effective emission area A we employ the method of Zhu *et al.*:[73] for $Z \ll 2R$ it is approximated by $A = 2\pi RZ(2^{1/n}-1)$ with $n = (V/I)\mathrm{d}I/\mathrm{d}V$. The emission current density J is then given by $J = I/A$.

3. Results and discussion

3.1. Growth of films of aligned nanotubes

The thermal CVD setup described in the previous section can be employed to produce large arrays of aligned carbon nanotubes. Films of aligned nanotubes can be obtained in the co-deposition mode using $Fe(CO)_5$ as the iron source as well as in the two-step process in which iron is deposited first and the catalytic nanotube growth is carried out subsequently at a higher temperature. We will focus on the latter procedure, results obtained with the co-deposition technique are similar and have been presented in our initial report.[72]

Fig. 2 displays a scanning electron microscope (SEM) image of a film of aligned MWNT which was grown in a two-step process with carbon monoxide as buffer and carrier gas. Carbon monoxide is known as a carbon feedstock gas for growth of SWNT on supported metal particles[7] and in the gas phase.[20,21] At the relatively low CVD temperature of 750 °C, however, the SWNT production rate from CO is small. In addition, our catalyst preparation procedure does not provide particles of sufficiently small diameters in the range of 1 nm on the substrate (see below). Thus we do not observe SWNT but only MWNT. The aligned nanotube film is characterised by a large degree of homogeneity, as can be seen from Fig. 2a which displays approx. 20 mm^2 of film surface. At various positions the films contains cracks, shown enlarged in part b) of the figure. Here the alignment of the nanotubes is visible. The nanotube film surface is displayed in high magnification in Fig. 2c. It appears as an entangled nanotube mat, not as an array of nanotube ends. This reflects the fact that the nanotubes are only roughly aligned with considerable disorder on a short length scale. Fig. 3 depicts two SEM images of an aligned nanotube film which was obtained under similar conditions but with argon as buffer and carrier gas instead of CO. Some nanotube film edges are displayed, showing clearly the rough alignment of the nanotubes and their orientation perpendicular to the substrate surface. It is apparent that carbon nanotubes are by far the predominant reaction product, the fraction of contamination with non-tubular material is very small. The film morphology is very similar to that shown in Fig. 2, providing additional evidence that use of CO as buffer and carrier gas has no impact on the MWNT growth process. The length of the nanotubes is on the order of a few tens of μm. We have not yet studied the nanotube growth rate. The aligned nanotube films reported here are structurally similar to films produced by other variations of the thermal CVD technique[28,35,36,39] or—on a shorter length scale—to bundles of aligned nanotubes.[30,32,33] Our nanotube production process has the advantage that in contrast to other methods the catalyst is prepared *in situ*. As a consequence, no additional and potentially complicated substrate preparation steps like metal deposition in a separate apparatus are necessary. In addition, only very common precursor materials are used which allow continuous operation of the process. Other more involved procedures or processes making use of less common solid organometallic precursors, may on the other hand result in better alignment of the nanotubes.[74] Considerably better alignment can be achieved in plasma assisted CVD processes[50–54] where the electrical self-bias field results in the relative alignment of the nanotubes.[55] No electric field is present in the thermal CVD processes like the one presented here. It is very likely that the observed alignment simply stems from a steric effect: the high nanotube nucleation density on the substrate allows only one preferential growth direction for the nanotubes, perpendicular to the substrates. If the nucleation density and the growth rate become too small, no alignment is observed.

In Fig. 4, two transmission electron microscopy (TEM) pictures of nanotube material which was prepared in the co-deposition mode and scratched off the silicon substrate are shown. In the low magnification image MWNT of a narrow diameter distribution around 23 nm are visible. The alignment of the nanotubes is preserved despite the sonication process of the material during the preparation of the TEM samples. At a few locations dark spots are visible, corresponding to metal or metal carbide inclusions in the nanotubes. No graphitic by-

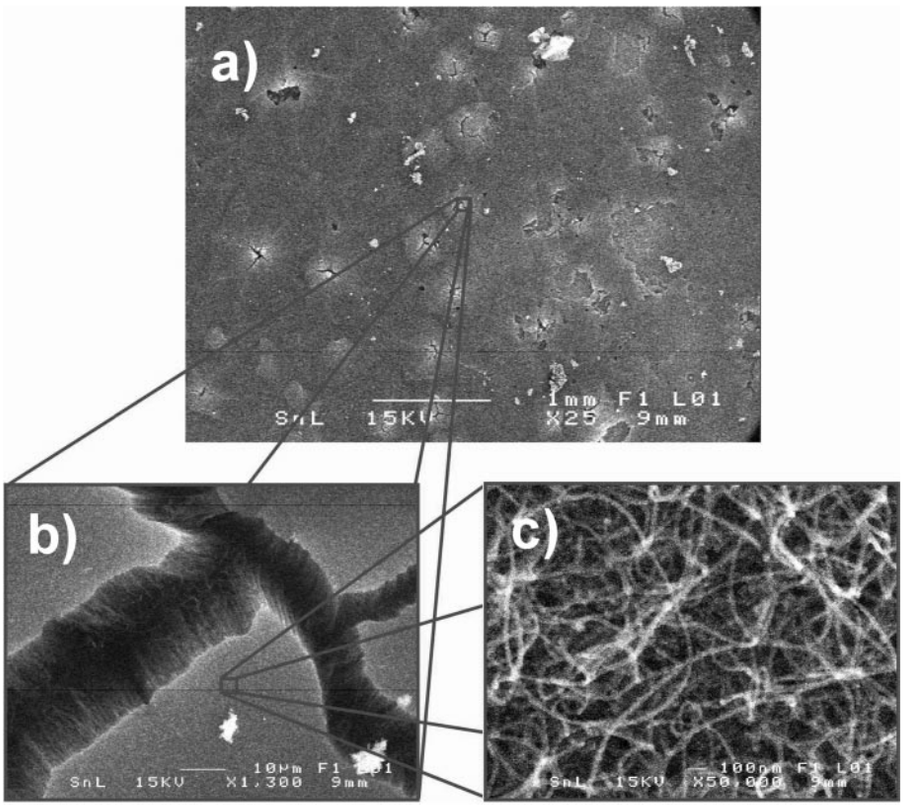

Fig. 2 SEM images of a film of aligned carbon nanotubes on silicon at three different magnifications. The film was obtained in a two-step process with CO as buffer and carrier gas. 1. Iron deposition: CO flow 600 sccm, CO flow through the carbonyl bubbler 8 sccm, temperature 200 °C, duration 40 minutes. 2. Nanotube CVD: CO flow 600 sccm, H_2 100 sccm, C_2H_2 5 sccm, temperature 750 °C, duration 3 hours. a) Low magnification image showing the homogeneous film, b) higher magnification image showing a crack in the film, c) high magnification image of the nanotube film surface.

products, typical for material produced by the arc-discharge method,[75] are visible. The nanotube surfaces appear to be relatively rough, indicating coverage with some amorphous carbon. The high magnification TEM micrograph in Fig. 4 reveals the multilayer tubular structure of the product. In this example, the hollow core of the nanotube is partially filled with iron or iron carbide. This observation can be explained if the catalyst particle is in a liquid state during the nanotube growth process, as also inferred by others[76] from similar results. An alternative interpretation would be enhanced surface diffusion of iron at the elevated temperature of the nanotube production process. The nanotube in the figure shows a relatively large defect density, evident as discontinuities in the carbon layer structure. CVD-grown MWNT are known to be structurally less perfect than those obtained from an arc-discharge process. However, we observed structural changes with loss of graphitisation on a minute timescale during imaging of the material in the TEM. This can be attributed to the electron–nanotube interaction in the electron microscope. Thus defects in the nanotube of Fig. 4 can only partially be attributed to the growth process.

3.2. Formation of metal particles as nucleation sites on the substrate

The formation of metal particles on the Si substrates was studied *ex situ* using atomic force microscopy (AFM). First, an iron film was deposited at 200 °C as in the nanotube production runs described above, but the substrate was then removed from the production furnace for AFM inspection. A typical image of such a film is depicted in Fig. 5a. Its thickness was not determined directly. It can be approximated very roughly by assuming homogeneous iron deposition all along the hot zone of the furnace beyond the cold injector. Under the conditions of the experiments (see caption of Fig. 5) a nominal film thickness of 50 nm is obtained. In reality, however, the iron film thickness on the substrate is considerably larger since the iron deposition is not homogeneous as assumed for the thickness estimation. Visibly more deposition occurs in the region of the substrate a few centimetres beyond the cold injector. The surface of the film appears to be very smooth, with the surface roughness being considerably smaller than 10 nm. Only a few particles are visible. The same film was transferred back into the CVD apparatus and heated to 750 °C in a CO–H_2 flow. The high temperature was held constant for 30 minutes, before the furnace was cooled again. No carbon feedstock gas was added and thus no carbon nanotubes were grown. However, the morphology of the iron film changed considerably, as can be seen in the AFM picture of Fig. 5b, taken after this procedure. A dense film of hemispherical structures with diameters of some tens of nanometres is visible. The diameters of these particles are very similar to the diameters of the MWNT grown in the process described above. It is therefore apparent that a very dense film of metal nucleation sites is formed during heating of the as-deposited iron film.

In addition to nanometre-sized particles, also larger particles with diameters of some hundreds of nanometres are formed in the heating process. This is shown in the SEM images of Fig. 6a and b. They display an iron film, which was deposited under similar conditions as those in Fig. 5 but with a longer deposition duration, after heating at 750 °C for 30 minutes. The SEM pictures do not resolve particles with diameters of a few tens of nanometres. However, a dense and homogeneous film of larger particles (or islands) with diameters of some hundred nanometres is visible. The same film was exposed to nanotube growth conditions in a second step, resulting in the formation of non-aligned MWNT, shown in parts b) and d) of the figure. Large particles like those seen in Fig. 6 do not catalyse MWNT growth. It can not be excluded that these

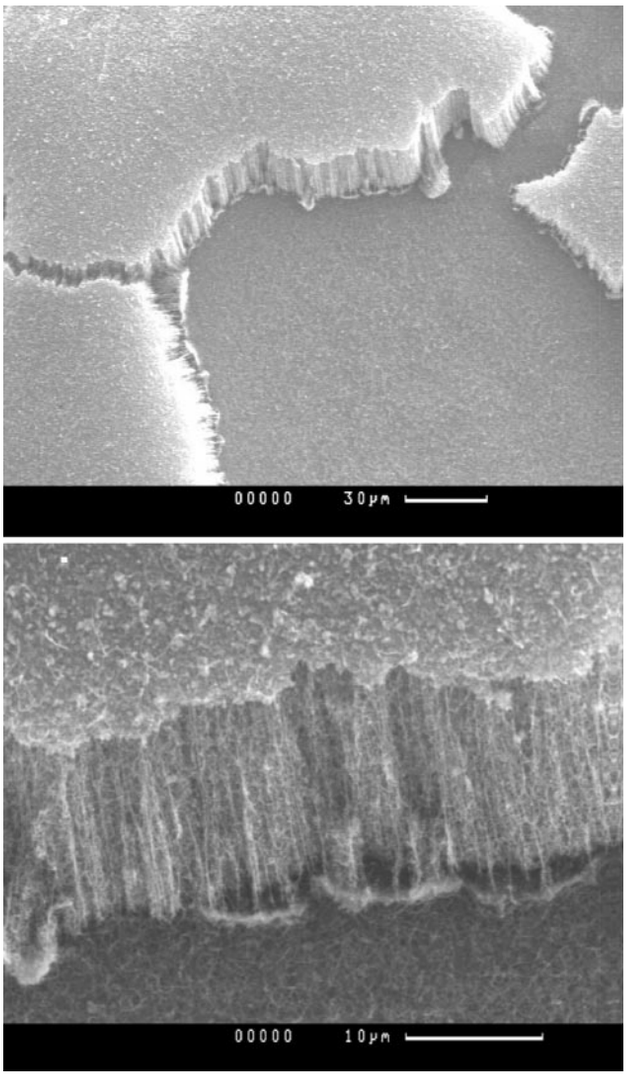

Fig. 3 SEM images of a film of aligned carbon nanotubes on silicon. The film was obtained in a two-step process with Ar as buffer and carrier gas. 1. Iron deposition: Ar flow 600 sccm, Ar flow through the carbonyl bubbler 5 sccm, temperature 200 °C, duration 20 minutes. 2. Nanotube CVD: Ar flow 600 sccm, H_2 100 sccm, C_2H_2 5 sccm, temperature 750 °C, duration 3 hours. The pictures demonstrate the alignment of the nanotubes as well as the orientation perpendicular to the substrate.

particles are covered with smaller iron particles in the diameter range suitable for nucleation of nanotube growth similar to those in Fig. 5. However, the observation of a relatively low nanotube density obtained on this particle film suggests that the nucleation site density is considerably smaller than on catalyst films which enable growth of aligned nanotube films.

3.3. Model for aligned nanotube growth

The mechanism leading to the metal-catalysed formation of carbon nanotubes has been discussed widely in the literature (for a review, see ref. 6) and is similar to the catalysed growth of carbon fibres, investigated by Baker and co-workers three decades ago.[77] A transition metal particle catalyses the disproportionation of the hydrocarbon molecules (or, in the case of the Boudouard reaction, CO). Carbon atoms diffuse through the metal particle, potentially driven by a thermal gradient which arises from the exothermicity of the dissociation reaction of the hydrocarbon, and precipitate at the opposite end of the metal particle. The outer diameter of the nanotube is determined by the diameter of the metal particle. This model is in agreement with the similarity in the diameter distributions of

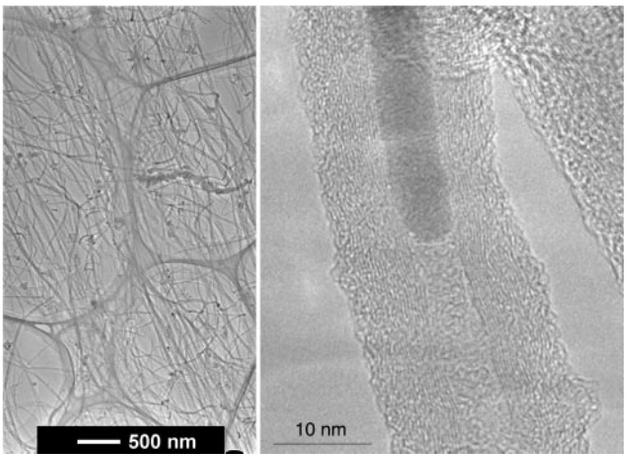

Fig. 4 TEM images of MWNT material grown on a Si wafer during co-deposition of iron and carbon at 750 °C. Flow conditions were as in the CVD step of Fig. 3 except that iron pentacarbonyl was also added by feeding 5 sccm Ar through the bubbler. A portion of the nanotube film was scratched off the substrate and dispersed in methanol assisted by ultrasonication. A drop of the dispersion was put on a holey carbon film on a copper TEM grid. Both images were recorded with 200 keV electron energy.

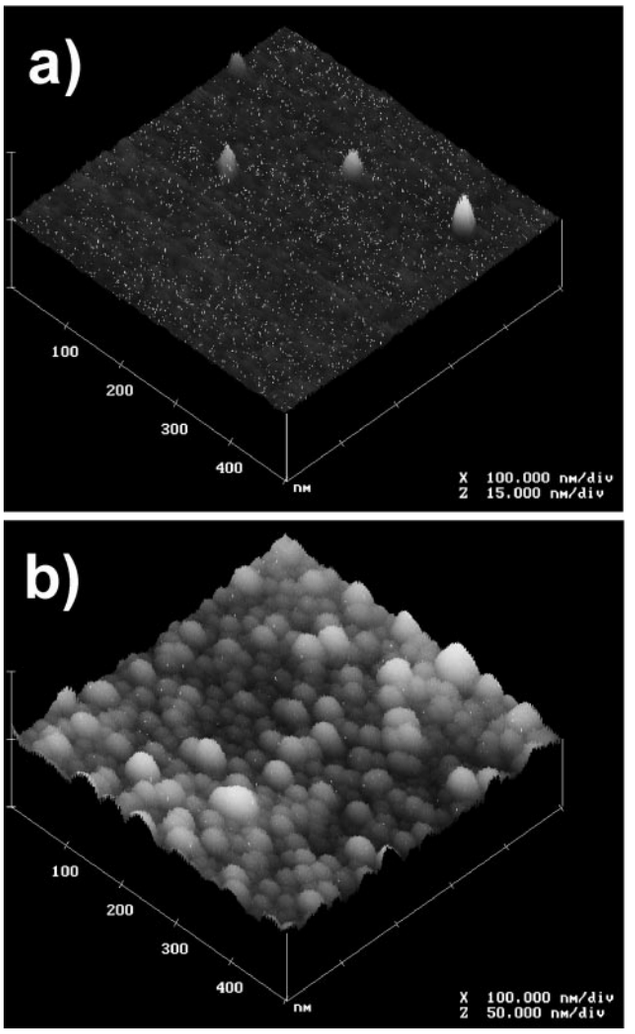

Fig. 5 Tapping-mode AFM images of an as-deposited iron film (a) and the same film after heating in an $Ar–H_2$ mixture at 750 °C for 30 minutes (b). The iron film was grown at 200 °C with CO as buffer and carrier gas, total flow 600 sccm, 5 sccm CO through the carbonyl bubbler, duration 10 minutes.

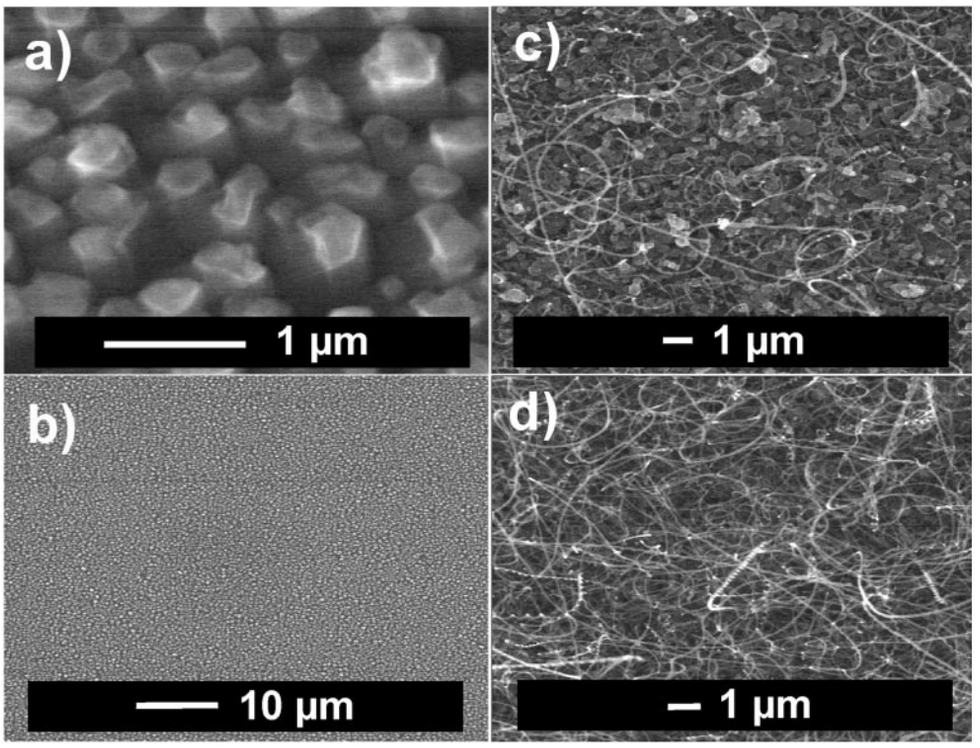

Fig. 6 a)+b): SEM images of an iron film after heating in an Ar–H_2 flow (600 : 100 sccm) at 750 °C for 30 minutes. Iron was deposited from $Fe(CO)_5$ at 200 °C with Ar as buffer and carrier gas, total flow 600 sccm, 8 sccm Ar through the carbonyl bubbler, duration 40 minutes. Large particles of some hundred nanometre diameter are formed. c)+d): The same film after CVD growth of carbon nanotubes in an Ar–H_2–C_2H_2 atmosphere. Growth conditions were: Ar 600 sccm, H_2 100 sccm, C_2H_2 5 sccm, temperature 750 °C, duration 3 hours. Non-aligned MWNT are formed. The two images were taken at different positions of the substrate, showing different nanotube densities.

nanotubes, Fig. 4, and metal particles, Fig. 5, as well as with the sizes of the metal particle inclusions seen in the TEM images of Fig. 4. We have no further probe available to check for the microscopic growth model, but the similarity of the nanotube growth process described here and those which led to the development of the above-mentioned model suggests that the same mechanism governs nanotube formation here.

Two possibilities for the growth direction of the nanotube relative to the metal particle exist, both having been observed experimentally in thermal and plasma-assisted CVD processes:

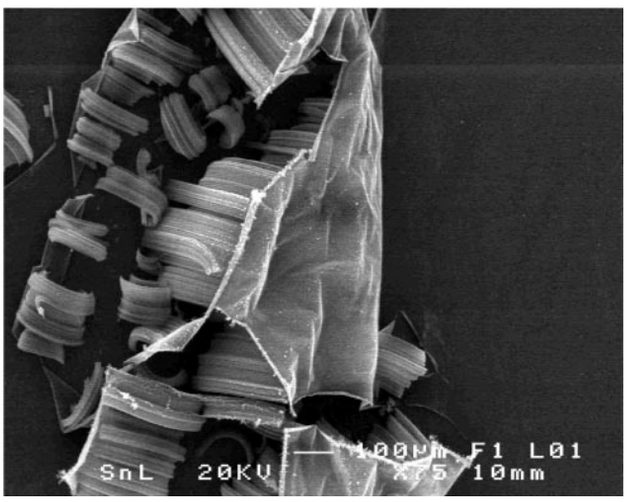

Fig. 7 SEM image of an incompletely formed film of aligned nanotubes. Iron was pre-deposited at 200 °C for 20 minutes with CO as buffer and carrier gas (600 sccm), 8 sccm CO through the carbonyl bubbler. CVD was carried out at 750 °C for 1 hour in a CO—H_2–C_2H_2 atmosphere with CO 600 sccm, H_2 100 sccm, C_2H_2 5 sccm. Growth of aligned nanotubes occurred incompletely. Apparently the continuous metal film covering the substrate has been lifted up by the growing nanotubes, indicating the tip-growth mechanism.

(1) the particle remains adsorbed on the substrate during nanotube growth (bottom growth);[37,39,52,54] (2) the particle is lifted up from the substrate by the growing nanotube (tip growth).[35,51,78] Occasionally, nanotubes which show metal encapsulations along longer portions of their length are observed, leading to modified growth scenarios, *e.g.* ref. 50. In the present study, the question of whether bottom or tip-growth prevails can be answered by looking at an incompletely grown aligned nanotube film, depicted in Fig. 7. The bundles of aligned nanotubes which formed on the substrate are covered with a metal film which continues on the substrate where no nanotubes are present. This film is absent close to the bottom ends of the long (approx. 100 µm) nanotubes. This indicates that the film has been lifted up by the growing nanotubes as a consequence of the tip-growth mechanism. The lifted film appears to be relatively thick.

We summarise the process leading to the formation of films of aligned nanotubes by the cartoon in Fig. 8. Deposition of iron atoms at 200 °C leads to the formation of a smooth iron film. Heating in the reducing atmosphere leads to particle formation with particle diameters of some tens of nanometres. These particles nucleate carbon nanotube growth at the CVD temperature in the presence of the hydrocarbon gas, here acetylene. They are lifted up from the substrate due to the tip-growth mechanism.

3.4. Simple procedure to obtain roughly horizontally aligned nanotubes

A large body of information on aligned nanotube growth perpendicular to the substrate surface is available. This is not the case for formation of horizontally aligned nanotubes, either free-standing or parallel to a substrate. Freestanding films of aligned SWNT can be obtained by filtration and deposition in a strong magnetic field.[79] Hot filament plasma CVD can be employed to grow aligned nanotubes with an orientation of 45° relative to the substrate plane, while an aligned nanotube film

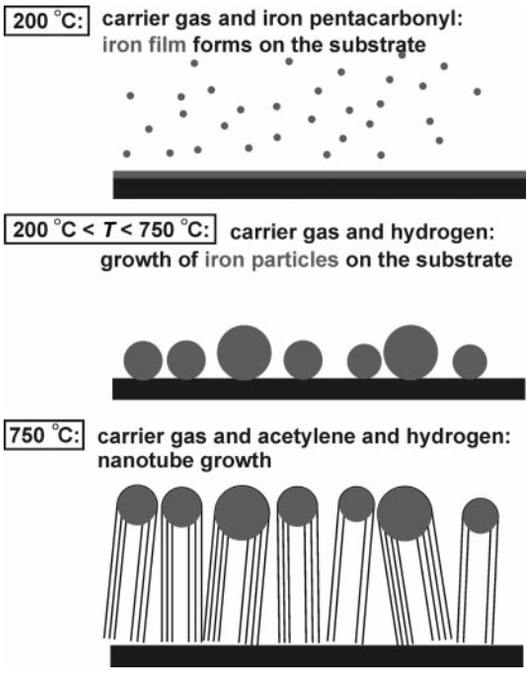

Fig. 8 Schematic picture of the processes leading to the formation of films of aligned nanotubes in the present study. Three steps can be distinguished: iron film growth, particle formation and nanotube nucleation and film growth in the tip-growth mode.

parallel to the surface is obtained by rolling a Teflon rod over such an inclined film.[57] We observed that a simple mechanical procedure leads to a rough horizontal alignment of the nanotubes grown in the two-step process (Fe deposition and thermal CVD) described above. The upper part of Fig. 9 displays a SEM picture of such a nanotube film. The end of a pair of tweezers was carefully drawn through the centre of the film, resulting in the wide trench in the film. The higher magnification image of the figure reveals that the bottom of this trench is covered with carbon nanotubes which are roughly aligned and oriented parallel to the substrate surface. Thus a simple mechanical procedure leads to the horizontal alignment of carbon nanotubes, starting from an unoriented nanotube film. We have not tried to optimise this method, but we are confident that such efforts can also provide the means to obtain large-area horizontally aligned nanotubes.

3.5. Non-aligned nanotube films grown from CH_4

The nanotube films discussed so far were synthesised using acetylene as carbon feedstock gas. The advantage of the use of acetylene is a relatively low nanotube growth temperature, in our experiments 750 °C. Furthermore, it has been inferred from the present results, in agreement with studies in the literature,[28,36] that the catalytic decomposition process occurs at a sufficiently high rate to allow formation of aligned carbon nanotube films without the necessity of using a pre-treated or porous substrate material which would supply a certain template for the nanotube growth direction. A disadvantage of acetylene is its tendency to form self-pyrolysis products at temperatures and pressures which are sufficiently high for nanotube growth. The corresponding unwanted by-products form amorphous carbon contaminations, reducing the nanotube purity. An alternative carbon feedstock gas for which the problem of self-pyrolysis is significantly reduced is methane, CH_4. Methane is the most prominent precursor for thermal CVD production of SWNT.[9–12] Presumably, the relatively low catalytic decomposition rate of methane favours the encapsulation of larger metal particles, while very small metal particles in the range of one nanometre can nucleate the formation of SWNT.[7,20] The formation of MWNT from methane in *thermal*

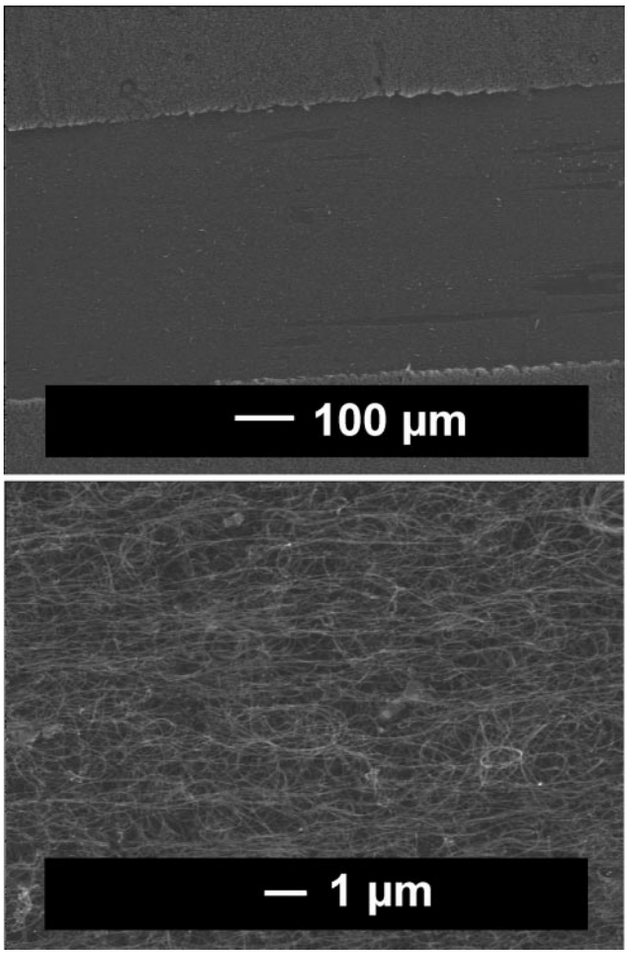

Fig. 9 SEM images of a mechanically obtained horizontally aligned carbon nanotube film. The upper image shows, in low magnification, the trench through the original nanotube film which was obtained by gently drawing a pair of tweezers through the film. The trench is displayed in higher magnification in the lower image, revealing the rough alignment of the nanotubes parallel to the substrate plane. The nanotube film was synthesised on a pre-deposited iron film at 750 °C, flow conditions as in Fig. 3, CVD duration 1 hour.

catalytic CVD processes has only been observed in processes where solid metal oxide solutions were reduced in an H_2–CH_4 atmosphere.[80,81] Plasma CVD processes often employ CH_4 for the synthesis of (aligned) MWNT films.[47,48,50,56,57] Nanotubes produced by CVD of methane are generally characterised by a high degree of purity due to the low self-pyrolysis rate. The properties of the third most simple hydrocarbon molecule, ethylene (C_2H_4), are positioned somewhere in between those of acetylene and methane with respect to its function as carbon nanotube precursor gas.[7,8,22,39]

We studied the formation of nanotubes from methane using the same procedure as described above with acetylene replaced by methane. Fig. 10 shows a nanotube film obtained at a growth temperature of 1100 °C on a pre-deposited iron film. The film is dense and consists of non-aligned MWNT with lengths of several micrometres and diameters of some tens of nanometres. Despite the much higher processing temperature compared to the CVD growth from acetylene, the material appears to be impurity-free. SWNT are not observed. The processing temperature is somewhat higher than in the studies reporting SWNT growth from methane[9–12] which lie between 900 and 1000 °C. Our method of metal catalyst preparation can not be expected to result in efficient formation of metal particles with sufficiently small diameters for SWNT nucleation (see section 3.2). The high CVD temperature increases the

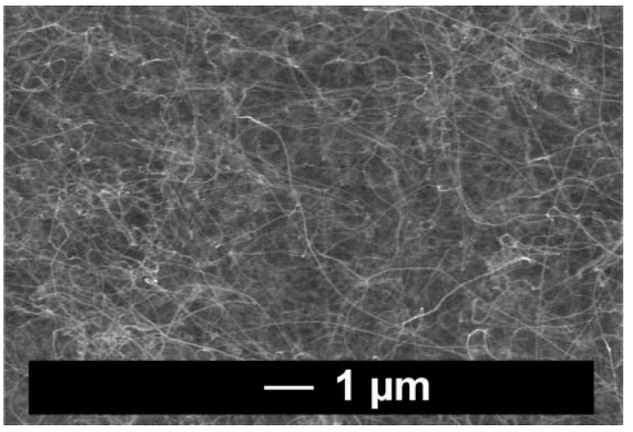

Fig. 10 SEM image of a film of MWNT synthesised by thermal CVD of methane. Iron was pre-deposited at 200 °C in flowing Ar (600 sccm), 8 sccm Ar through the carbonyl bubbler. CVD was carried out at 1100 °C for 15 minutes, with Ar 500 sccm, CH_4 13 sccm, H_2 100 sccm.

decomposition rate and thus the precipitation rate of solid carbon. It can therefore be expected that the tendency for encapsulation of larger metal particles with graphitic carbon is reduced compared to lower processing temperatures, allowing efficient production of MWNT.

At a somewhat lower CVD temperature short duration CVD processes involving methane can be used to synthesise low density nanotube films with short length nanotubes. This is demonstrated in Fig. 11, which displays two SEM images of nanotube films synthesised at 1050 °C with a CVD duration of 25 seconds (top) and 50 seconds (bottom). The film in the upper image consists of isolated nanotubes of a few hundred nanometres length with very low density. Increasing the CVD duration leads to a considerably higher nanotube density, as seen in the lower image, while the average nanotube length remains very short. The increase in the nanotube density could indicate that some metal particles nucleate nanotubes delayed compared to others.

All the nanotube growth experiments discussed so far were carried out in the presence of both hydrocarbon gas and hydrogen. The main role of hydrogen is to reduce the deposited iron catalyst which might become partially oxidised in the absence of hydrogen. In order to observe the role of hydrogen during the CVD process we carried out the two-step nanotube synthesis by first depositing an iron film as before followed by heating in an argon–hydrogen atmosphere which keeps the iron catalyst particles reduced. After the nanotube growth temperature of 1100 °C had been reached, the hydrogen supply was shut off before CH_4 was added and nanotube CVD growth was carried out. Fig. 12 shows the result of this procedure for different durations of the CVD process. In the case of the 1 minute process, a dense film of MWNT is formed with micrometre-long nanotubes of approx. 35 nm diameter. When the duration of the CVD process is increased to 5 minutes, a thickening of the nanotubes is observed, forming fibres with some hundred nanometres diameter. This becomes more drastic when the CVD step is carried out for 20 minutes. In this case, a dense film of quasi-vertically aligned carbon fibres with diameters around 5.5 µm is formed. Such a thickening effect is not observed if CVD is carried out in the presence of hydrogen.

The thickening is probably due to a non-catalytic decomposition of methane on the nanotube or fibre surfaces. The equilibrium of the disproportionation reaction $CH_4 \rightarrow C + 2H_2$ will shift to the left side if hydrogen is added, thus limiting the efficiency of the non-catalytic formation of carbon. The impact of the presence of hydrogen on the catalyst, however, can not be inferred from these observations. Peigny *et al.* have studied

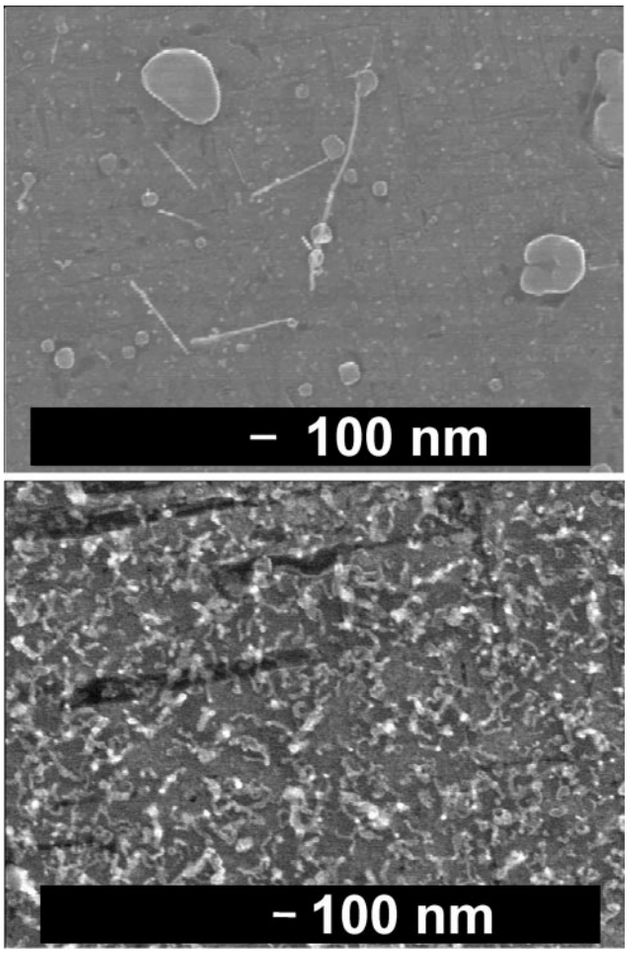

Fig. 11 SEM images of MWNT grown from CH_4 in short CVD processes. Growth conditions as in Fig. 10 except CVD temperature (1050 °C). Duration of CVD growth: 25 s (top), 50 s (bottom).

the influence of the H_2–CH_4 flow ratio on the formation of nanotubes in solid solutions.[81] They found a maximum carbon nanotube quality at a molar methane–iron ratio around 14%, while the carbon nanotube growth rate was highest at 24%. For larger CH_4–H_2 ratios, the relative amount of non-tubular carbon increases. Our results agree with these observations. It should be noted, however, that the method of Peigny *et al.* predominantly results in the formation of thin MWNT with a only a few carbon layers and that they do not observe a pronounced thickening effect during a one hour CVD time at 1050 °C.

In closing this section we will suggest a way towards simple production of carbon nanotube patterns. We observed that carbon nanotube growth from CH_4 at 1100 °C is inhibited if a thin (5 nm) layer of Ti is deposited on the Si wafer before the usual iron pre-deposition followed by nanotube CVD synthesis is carried out. This is demonstrated in Fig. 13, showing the result of a nanotube growth experiment on a partially Ti-coated Si wafer. Nanotubes are only formed on the part of the Si wafer which is not coated with Ti. Thus, patterning of a substrate with Ti using a mask technique or electron beam lithography should allow the growth of carbon nanotube patterns by the described CVD technique. In contrast to our results it was reported that MWNT can be obtained by thermal CVD from C_2H_2 at 660 °C on a Ti–Fe 10 nm–5 nm double-layer,[29] while CVD from C_2H_4 on iron-coated Ti substrates between 700 and 775 °C results in formation of aligned TiC-filled nanotubes.[82] Currently we can only speculate about possible reasons for the discrepancy between these and our observations. Compared to the two mentioned studies,[29,82] in

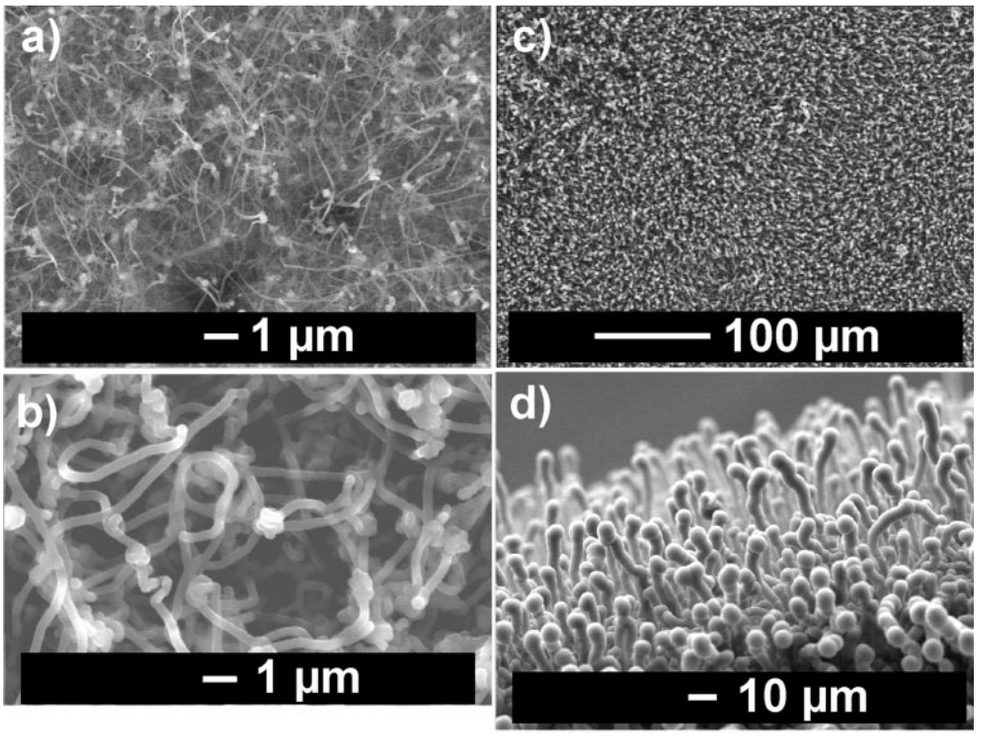

Fig. 12 SEM images demonstrating the thickening of MWNT and fibres obtained by a CVD process in the absence of hydrogen. For all samples shown, an iron film was pre-deposited for 30 minutes at 200 °C in flowing Ar (conditions as in Fig. 10). After iron deposition, the furnace was heated to 1100 °C with a flow of 600 sccm Ar and 100 sccm H_2. The H_2 was shut off when the final temperature was reached before a flow of 13 sccm CH_4 was added. CVD duration: a) 1 min, b) 5 min, c) and d) (showing same film) 20 min.

our experiment the Ti concentration is lower and the processing temperature higher. The lower Ti/Fe ratio (nominal 20% assuming homogeneous iron deposition but probably much smaller, see section 3.2) could result in the formation of a catalytically inactive Fe–Ti compound.

3.6. Nanotube growth on iron nitrate impregnated substrates and field emission properties

Fig. 14 displays two SEM images of carbon nanotube films which were synthesised by CVD on an iron film which was

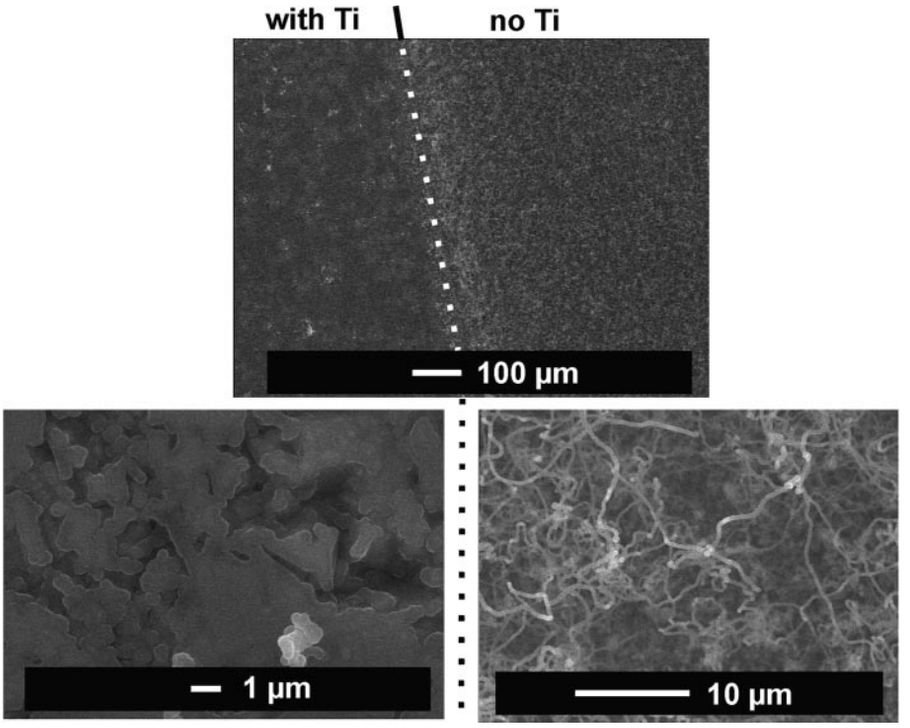

Fig. 13 Suppression of nanotube growth by a pre-deposited Ti film. Before iron deposition and CVD, a 5 nm thick Ti film was deposited on the Si wafer by electron beam sputter coating. A corner of the wafer was left uncoated by masking it during the Ti deposition process. The so-treated Si wafer was then used as a substrate for nanotube film growth. Iron pre-deposition was carried out at 200 °C for 5 min in 600 sccm Ar with 5 sccm Ar through the carbonyl bubbler. CVD occurred at 1100 °C in 600 sccm Ar, 100 sccm H_2 and 10 sccm CH_4. The upper SEM image shows the interface between Ti-coated area (left) and uncoated area (right). Nanotubes are only formed in the area where no Ti was deposited, as can be seen in the two higher magnification SEM images taken in the corresponding regions.

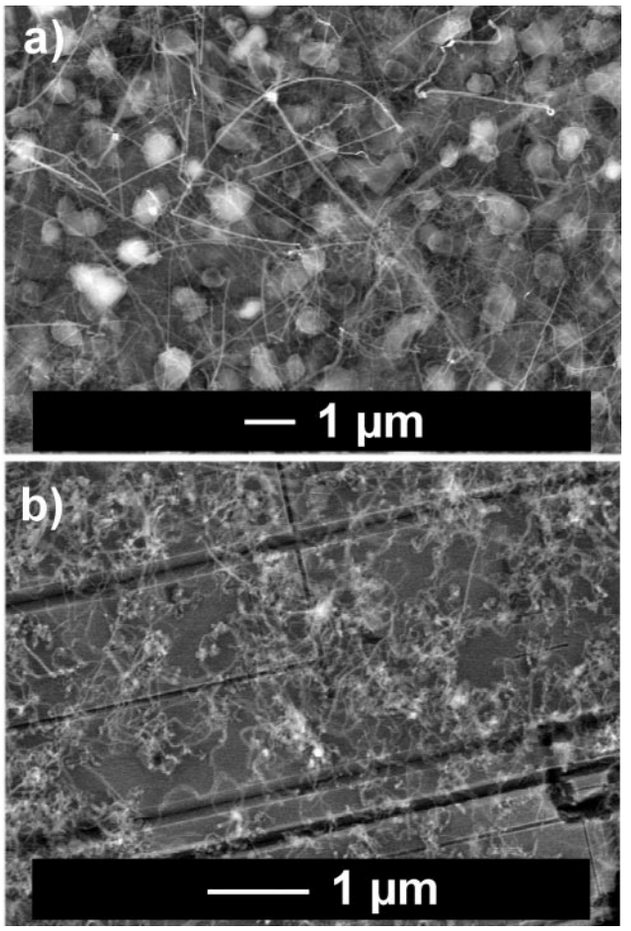

Fig. 14 SEM images of MWNT films grown on Si wafers after impregnation with $Fe(NO_3)_3{\cdot}9H_2O$. Upper image: Rapid evaporation of the solvent by vacuum pumping, creating a relatively thick iron film, followed by CVD at 1050 °C for 5 minutes with CH_4 as carbon feedstock. Gas flow composition: Ar 600 sccm, CH_4 13 sccm, H_2 100 sccm. Lower image: Iron nitrate solution removed with an air gun, Si wafer washed with de-ionised water and dried in air, creating a very thin, optically invisible catalyst coating. CVD was carried out under the same conditions as before but for 30 minutes.

obtained by impregnation of the Si substrates with $Fe(NO_3)_3{\cdot}9H_2O$. The film in the upper image was grown on a thick iron catalyst film which formed a pattern of large particles, visible underneath the nanotubes, while the lower film was obtained by CVD on a thin catalyst film which is not visible in the SEM image. The duration of the CVD growth was five minutes for the upper film and 30 minutes for the lower with the remaining growth parameters being identical. The nanotubes in the upper image have lengths in the micrometre range, typical diameters of 35 nm and are quite straight. The nanotube film they make up is rather thin, exposing the underlying substrate. The nanotubes in the lower image appear surprisingly shorter than those in the upper image despite the longer CVD process they were obtained with. They have smaller diameters, around 12 nm, and are less straight. The reduced straightness makes a estimation of the true nanotube length difficult and thus also the comparison with the nanotube material obtained on the thick iron film in the shorter process. More interesting is the observation of smaller nanotube diameters in the lower image material. It provides evidence for the presence of smaller diameter iron particles in the thin iron film since the diameter of a catalyst particle is believed to determine the diameter of the MWNT it nucleates. This explanation is plausible also in the light of the observation of small diameter MWNT and SWNT obtained in iron-catalysed thermal CVD processes with small average metal particle sizes.[81] The nanotubes from the long-duration CVD process appear to be less clean than the short CVD duration material. This is obviously due to pyrolytic formation of non-tubular carbon from CH_4 and could possibly be prevented by a shorter CVD duration or a different H_2–CH_4 flow ratio.

As mentioned in the introduction, field emission from carbon nanotube films is relevant for several potential technical applications. Thus a number of studies has been devoted to the investigation of the electron emission efficiency from films of MWNT[57,58,83–89] and SWNT.[73,83,89,90] High electron emission efficiencies and low threshold fields for electron emission from such films were demonstrated. We measured the field emission properties of the MWNT film displayed in the upper part of Fig. 14. The corresponding field emission current density–voltage dependence is shown in Fig. 15. Electron emission starts to occur at electric fields between 5 and 6 V μm^{-1}, reaching values of several mA cm^{-2} for larger fields.

The inset in Fig. 15 shows a Fowler–Nordheim (F–N) plot of the same data. According to the theory for field emission the current density J is given by

$$J \propto E^2 \exp\left[-\frac{6.83\times10^9\phi^{3/2}}{E}\right] \quad (1)$$

ϕ is the work function of the cathode material (in the present case the nanotubes) in electronvolts. Its value has been determined in energy dispersive field emission measurements by Gröning *et al.* to be 5 eV for the case of MWNT.[83] E is the *local* electric field (in V m^{-1}) which is related to the applied macroscopic field $F = V/d$ by $E = cF$ with c being the field enhancement factor, V the applied voltage drop and d the nanotube film–anode distance. A plot of $\ln(J/F^2)$ *versus* $1/F$ should therefore result in a linearly decreasing curve. Our field emission data decrease linearly in the F–N plot, demonstrating that indeed field emission is the reason for the measured current. Some deviations from the linear functional form are observed for very small and very large fields, probably due to the detection limit of our experimental setup and due to possible saturation effects, respectively. Three consecutive voltage scans are plotted in Fig. 15. They show identical slopes in the F–N plot, indicating that the field enhancement factor c does not change with the number of voltage scans. A value of approx 2700 can be determined for c from the slope. This is close to values reported in the literature for MWNT[58,83,87] and SWNT.[90]

Commonly used figures of merit which characterise the efficiency of field emitters are the turn-on field F_{to} and the

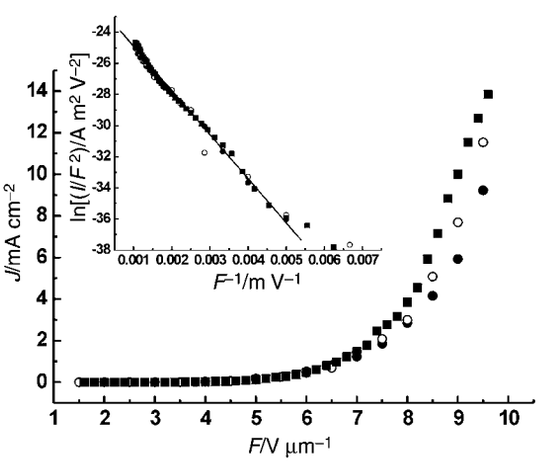

Fig. 15 Electron field emission from the MWNT film displayed in the upper part of Fig. 14. The inset shows the Fowler–Nordheim plot of the corresponding data. Full circles, empty circles and full squares: 1st, 2nd and 3rd voltage scan, respectively. The line in the Fowler–Nordheim plot is a least-squares fit to the 3rd voltage scan.

threshold field F_{th} at which the current densities exceed $10\ \mu A\ cm^{-2}$ and $10\ mA\ cm^{-2}$, respectively. For the data plotted in Fig. 15 these characteristic field strengths are $F_{to} = 4.75\ V\ \mu m^{-1}$ and $F_{th} = 9\ V\ \mu m^{-1}$. These numbers are close to or slightly larger than values reported for both MWNT[86,88,89] and SWNT[73,89,90] films which were synthesised by various methods. The maximum emission current density of about $14\ mA\ cm^{-2}$ is achieved with a field of approx. $10\ V\ \mu m^{-1}$. In some studies where field emission from films of aligned MWNT was investigated considerably smaller threshold fields and larger maximum current densities were reported.[58,85] It has been discussed that the performance of a nanotube film cathode depends sensitively on the nanotube density.[84] The nanotube density in the film which is shown in Fig. 14a is rather low, in particular compared to films of aligned nanotubes, and might therefore be sub-optimal for field emission. It can still be stated that the CVD method presented here produces nanotube films of high electron emission efficiency. A slight increase of the electron emission efficiency is observed with increasing number of scans. This might be a training effect which is particular for our nanotube film material.

4. Conclusion

The thermal CVD methods presented here are capable of producing films of MWNT in simple processes. The versatility of the methods has been demonstrated by the various film morphologies which can be achieved by alternation of the growth conditions such as aligned and non-aligned nanotubes.

In this paper we could only show some general trends of the product–growth conditions dependence. There is clearly more to learn from more detailed studies of various aspects, such as the dependence of the nanotube structure and density on the hydrogen concentration during the reaction, critical values of catalyst film thickness for the nanotube film growth, substrate-induced growth effects, field emission properties as a function of nanotube length, diameter and nanotube film density, among many others. Investigations along these lines are underway in our laboratory.

Acknowledgements

Part of this work was supported financially by the Swedish Programme for Strategic Research (Stiftelsen för Strategisk Forskning, SSF) within the CARAMEL consortium. We are grateful to Prof. Eleanor Campbell for support and for valuable discussions. We thank Heinrich Riedl for experimental assistance.

References

1 R. Saito, G. Dresselhaus and M. S. Dresselhaus, *Physical properties of carbon nanotubes*, Imperial College Press, London, 1998.
2 W. A. de Heer and R. Martel, *Physics World*, 2000, **June**, 49.
3 S. J. Tans, A. R. M. Verschueren and C. Dekker, *Nature*, 1998, **393**, 49.
4 H. Dai, J. H. Hafner, A. G. Rinzler, D. T. Colbert and R. E. Smalley, *Nature*, 1996, **384**, 147.
5 C. Journet and P. Bernier, *Appl. Phys. A*, 1998, **67**, 1.
6 Ch. Laurent, E. Flahaut, A. Peigney and A. Rousset, *New J. Chem.*, 1998, **22**, 1229.
7 J. H. Hafner, M. J. Bronikowski, B. R. Azamian, P. Nikolaev, A. G. Rinzler, D. T. Colbert, K. A. Smith and R. E. Smalley, *Chem. Phys. Lett.*, 1998, **296**, 195.
8 J.-F. Colomer, G. Bister, I. Willems, Z. Konya, A. Fonseca, G. Van Tendeloo and J. B. Nagy, *Chem. Commun.*, 1999, 1343.
9 J.-F. Colomer, C. Stephan, S. Lefrant, G. Van Tendeloo, I. Willems, Z. Kónya, A. Fonseca, Ch. Laurent and J. B. Nagy, *Chem. Phys. Lett.*, 2000, **317**, 83.
10 J. Kong, H. T. Soh, A. M. Cassell, C. F. Quate and H. Dai, *Nature*, 1998, **395**, 878.
11 A. M. Cassel, J. A. Raymakers, J. Kong and H. Dai, *J. Phys. Chem. B*, 1999, **103**, 6484.
12 M. Su, B. Zheng and J. Liu, *Chem. Phys. Lett.*, 2000, **322**, 321.
13 N. R. Franklin and H. Dai, *Adv. Mater.*, 2000, **12**, 890.
14 H. Dai, A. G. Rinzler, P. Nikolaev, A. Thess, D. T. Colbert and R. E. Smalley, *Chem. Phys. Lett.*, 1996, **260**, 471.
15 B. Kitiyanan, W. E. Alvarez, J. H. Harwell and D. E. Resaco, *Chem. Phys. Lett.*, 2000, **317**, 497.
16 E. Flahaut, A. Govindaraj, A. Peigney, Ch. Laurent, A. Rousset and C. N. R. Rao, *Chem. Phys. Lett.*, 1999, **300**, 236.
17 E. Flahaut, A. Peigney, Ch. Laurent and A. Rousset, *J. Mater. Chem.*, 2000, **10**, 249.
18 R. R. Bacsa, Ch. Laurent, A. Peigney, W. S. Bacsa, Th. Vaugien and A. Rousset, *Chem. Phys. Lett.*, 2000, **323**, 566.
19 H. M. Cheng, F. Li, G. Su, H. Y. Pan, L. L. He, X. Sun and M. S. Dresselhaus, *Appl. Phys. Lett.*, 1998, **72**, 3282.
20 K. Bladh, L. K. L. Falk and F. Rohmund, *Appl. Phys. A*, 2000, **70**, 317.
21 P. Nikolaev, M. J. Bronikowski, R. K. Bradley, F. Rohmund, D. T. Colbert, K. A. Smith and R. E. Smalley, *Chem. Phys. Lett.*, 1999, **313**, 91.
22 K. Hernadi, A. Fonseca, J. B. Nagy, D. Bernaerts and A. A. Lucas, *Carbon*, 1996, **34**, 1249.
23 Th. E. Müller, D. G. Reid, W. K. Hsu, J. P. Hare, H. W. Kroto and D. R. M. Walton, *Carbon*, 1997, **35**, 951.
24 A. Fonseca, K. Hernadi, P. Piedigrosso, J.-F. Colomer, K. Mukhopadhyay, R. Doome, S. Lazarescu, L. P. Biro, Ph. Lambin, P. A. Thiry, D. Bernaerts and J. B. Nagy, *Appl. Phys. A*, 1998, **67**, 11.
25 Á. Kukovecz, Z. Kónya, N. Nagaraju, I. Willems, A. Tamásu, A. Fonseca, J. B. Nagy and I. Kiricsi, *Phys. Chem. Chem. Phys.*, 2000, **2**, 3071.
26 I. Willems, Z. Kónya, J.-F. Colomer, G. Van Tendeloo, N. Nagaraju, A. Fonseca and J. B. Nagy, *Chem. Phys. Lett.*, 2000, **317**, 71.
27 J. M. Mao, L. F. Sun, L. X. Qian, Z. W. Pan, B. H. Chang, W. Y. Zhou, G. Wang and S. S. Xie, *Appl. Phys. Lett.*, 1998, **72**, 3297.
28 H. Kind, J.-M. Bonard, Ch. Emmenegger, L. O. Nilsson, K. Hernadi, E. Mailard-Schaller, L. Schlapach, L. Forro and K. Kern, *Adv. Mater.*, 1999, **11**, 1285.
29 Y. Y. Wei and G. Eres, *Nanotechnology*, 2000, **11**, 61.
30 K. Mukhopadhyay, A. Koshio, N. Tanaka and H. Shinohara, *Jpn. J. Appl. Phys.*, 1998, **37**, L1257.
31 K. Mukhopadhyay, A. Koshio, T. Sugai, N. Tanaka, H. Shinohara, Z. Konya and J. B. Nagy, *Chem. Phys. Lett.*, 1999, **303**, 117.
32 C. N. R. Rao, R. Sen, B. C. Satiskhumar and A. Govindaraj, *Chem. Commun.*, 1998, 1525.
33 B. C. Satishkumar, A. Govindaraj and C. N. R. Rao, *Chem. Phys. Lett.*, 1999, **307**, 158.
34 M. Terrones, N. Grobert, J. Olivares, J. P. Zhang, H. Terrones, K. Kordatos, W. K. Hsu, J. P. Hare, P. D. Townsend, K. Prassides, A. K. Cheetham, H. W. Kroto and D. R. M. Walton, *Nature*, 1997, **388**, 52.
35 R. Andrews, K. Jacques, A. M. Rao, F. Derbyshire, D. Qian, X. Fan, E. C. Dickey and J. Chen, *Chem. Phys. Lett.*, 1999, **303**, 467.
36 C. J. Lee, J. Park, S. Y. Kang and J. H. Lee, *Chem. Phys. Lett.*, 2000, **323**, 554.
37 C. J. Lee, J. H. Park and J. Park, *Chem. Phys. Lett.*, 2000, **323**, 560.
38 W. Z. Li, S. Xie, L. X. Qian, B. H. Chang, B. S. Zou, W. Y. Zhou, R. A. Zhao and G. Wang, *Science*, 1996, **274**, 1701.
39 S. Fan, M. G. Chapline, N. R. Franklin, T. W. Tombler, A. M. Cassel and H. Dai, *Science*, 1999, **283**, 512.
40 H. Kind, J.-M. Bonard, L. Forró, K. Kern, K. Hernadi, L.-O. Nilsson and L. Schlapbach, *Langmuir*, 2000, **16**, 6877.
41 H. Kanzow, A. Schmalz and A. Ding, *Chem. Phys. Lett.*, 1998, **295**, 525.
42 R. Sen, A. Govindaraj and C. N. R. Rao, *Chem. Mater.*, 1997, **9**, 2078.
43 R. Sen, A. Govindaraj and C. N. R. Rao, *Chem. Phys. Lett.*, 1997, **267**, 276.
44 S. Huang, L. Dai and A. W. H. Mau, *J. Phys. Chem. B*, 1999, **103**, 4223.
45 L. Biró, R. Ehlich, R. Tellgmann, A. Gromov, N. Krawez, M. Tschaplyguine, M.-M. Pohl, E. Zsoldos, Z. Vétesy, Z. E. Horáth and E. E. B. Campbell, *Chem. Phys. Lett.*, 1999, **306**, 155.

46 E. Czerwosz, P. Dluzewski, G. Dmowska, R. Nowakowski, E. Starnawska and H. Wronka, *Appl. Surf. Sci.*, 1999, **141**, 350.
47 L. C. Qin, D. Zhou, A. R. Kraus and D. M. Gruen, *Appl. Phys. Lett.*, 1998, **72**, 3437.
48 Q. Zhang, S. F. Yoon, J. Ahn, B. Gan, Rusli and M.-B. Yu, *J. Phys. Chem. Solids*, 2000, **61**, 1179.
49 Y. C. Choi, D. J. Bae, Y. H. Lee, B. S. Lee, I. T. Han, W. B. Choi, N. S. Lee and J. M. Kim, *Synth. Met.*, 2000, **108**, 159.
50 S. H. Tsai, C. W. Chao, C. L. Lee and H. C. Shih, *Appl. Phys. Lett.*, 1999, **74**, 3462.
51 Z. F. Ren, Z. P. Huang, J. W. Xu, J. H. Wang, P. Bush, M. P. Siegal and P. N. Provencio, *Science*, 1998, **282**, 1105.
52 Z. F. Ren, Z. P. Huang, D. Z. Wang, J. G. Wen, J. W. Xu, J. H. Wang, L. E. Calvet, J. Chen, J. F. Klemic and M. A. Reed, *Appl. Phys. Lett.*, 1999, **75**, 1086.
53 Z. P. Huang, J. W. Xu, Z. F. Ren, J. H. Wang, M. P. Siegal and P. N. Provencio, *Appl. Phys. Lett.*, 1998, **73**, 3845.
54 Ch. Bower, O. Zhou, W. Zhu, D. J. Werder and X. Jin, *Appl. Phys. Lett.*, 2000, **77**, 2767.
55 Ch. Bower, W. Zhu, S. Jin and O. Zhou, *Appl. Phys. Lett.*, 2000, **77**, 830.
56 O. Küttel, O. Groening, Ch. Emmenegger and L. Schalpbach, *Appl. Phys. Lett.*, 1998, **73**, 2113.
57 Y. Chen, D. T. Shaw and L. Guo, *Appl. Phys. Lett.*, 2000, **76**, 2469.
58 Y. Chen, S. Patel, Y. Ye, D. T. Shaw and L. Guo, *Appl. Phys. Lett.*, 1998, **73**, 2119.
59 O. R. Lourie, C. R. Jones, B. M. Barlett, P. C. Gibbons, R. S. Ruoff and W. E. Buhro, *Chem. Mater.*, 2000, **12**, 1808.
60 B. C. Satishkumar, A. Govindaraj, K. R. Harikumar, J.-P. Zhang, A. K. Cheetham and C. N. R. Rao, *Chem. Phys. Lett.*, 1999, **300**, 473.
61 R. Sen, B. C. Satishkumar, A. Govindaraj, K. R. Harikumar, M. K. Renganathan and C. N. R. Rao, *J. Mater. Chem.*, 1997, **7**, 2335.
62 M. Nath, B. C. Satishkumar, A. Govindaraj, C. P. Vinod and C. N. R. Rao, *Chem. Phys. Lett.*, 2000, **322**, 333.
63 S. L. Sung, S. H. Tsai, C. H. Tseng, F. K. Chiang, X. W. Liu and H. C. Shih, *Appl. Phys. Lett.*, 1999, **74**, 197.
64 M. Terrones, Ph. Redlich, N. Grobert, S. Trasobares, W.-K. Hsu, H. Terrones, Y.-Q. Zhu, J. P. Hare, C. L. Reeves, A. K. Cheetham, M. Rühle, H. W. Kroto and D. R. M. Walton, *Adv. Mater.*, 1999, **11**, 655.
65 M. Terrones, H. Terrones, N. Grobert, W. K. Hsu, Y. Q. Zhu, J. P. Hare, H. W. Kroto, D. R. M. Walton, Ph. Kohler-Redlich, M. Rühle, J. P. Zhang and A. K. Cheetham, *Appl. Phys. Lett.*, 1999, **75**, 3932.
66 R. Sen, B. C. Satishkumar, A. Govindaraj, K. R. Harikumar, G. Raina, J.-P. Zhang, A. K. Cheetham and C. N. R. Rao, *Chem. Phys. Lett.*, 1998, **287**, 671.
67 M. Terrones, A. M. Benito, C. Manteca-Diego, W. K. Hsu, O. I. Osman, J. P. Hare, D. G. Reid, H. Terrones, A. K. Cheetham, K. Prassides, H. W. Kroto and D. R. M. Walton, *Chem. Phys. Lett.*, 1996, **257**, 576.
68 J. Yu, J. Ahn, S. F. Yoon, Q. Zhang, Rusli, B. Gan, K. Chew, M. B. Yu, X. D. Bai and E. G. Wang, *Appl. Phys. Lett.*, 2000, **77**, 1949.
69 W. A. de Heer, A. Chatelain and D. Ugarte, *Science*, 1995, **270**, 1179.
70 J. M. Kim, W. B. Choi, N. S. Lee and J. E. Jung, *Diamond Relat. Mater.*, 2000, **9**, 1184.
71 Y. Saito and S. Uemura, *Carbon*, 2000, **38**, 169.
72 F. Rohmund, L. K. L. Falk and E. E. B. Campbell, *Chem. Phys. Lett.*, 2000, **328**, 369.
73 W. Zhu, C. Bower, O. Zhou, G. Kochanski and S. Jin, *Appl. Phys. Lett.*, 1999, **75**, 873.
74 Y. Yang, S. Huang, H. He, A. W. H. Mau and L. Dai, *J. Am. Chem. Soc.*, 1999, **121**, 10832.
75 T. W. Ebbesen, P. M. Ajayan, H. Hiura and K. Tanigaki, *Nature*, 1994, **367**, 519.
76 Y. Li, J. Chen, Y. Ma, J. Zhao, Y. Qin and L. Chang, *Chem. Commun.*, 1999, 1141.
77 R. T. K. Baker, *Carbon*, 1989, **27**, 315.
78 Z. W. Pan, S. S. Xie, B. H. Chang, L. F. Sun, W. Y. Zhou and G. Wang, *Chem. Phys. Lett.*, 1999, **299**, 97.
79 B. W. Smith, Z. Benes, D. E. Luzzi, J. E. Fischer, D. A. Walters, M. J. Casavant, J. Schmidt and R. E. Smalley, *Appl. Phys. Lett.*, 2000, **77**, 663.
80 A. Peigney, Ch. Laurent, F. Dobigeon and A. Rousset, *J. Mater. Res.*, 1997, **12**, 613.
81 A. Peigney, Ch. Laurent and A. Rousset, *J. Mater. Chem.*, 1999, **9**, 1167.
82 Y. Gao, J. Liu, M. Shi, S. H. Elder and J. W. Virden, *Appl. Phys. Lett.*, 1999, **74**, 3642.
83 O. Gröning, O. M. Küttel, Ch. Emmenegger, P. Gröning and L. Schlapbach, *J. Vac. Sci. Technol. B*, 2000, **18**, 665.
84 L. Nilsson, O. Groening, C. Emmenegger, O. Kuettel, E. Schaller, L. Schlapbach, H. Kind, J.-M. Bonard and K. Kern, *Appl. Phys. Lett.*, 2000, **76**, 2071.
85 A. M. Rao, D. Jacques, R. C. Haddon, W. Zhu, C. Bower and S. Jin, *Appl. Phys. Lett.*, 2000, **76**, 3813.
86 C. J. Lee, J. Park, S. Y. Kang and J. H. Lee, *Chem. Phys. Lett.*, 2000, **326**, 175.
87 A. N. Obraztsov, I. Pavlovsky, A. P. Volkov, E. D. Obraztsova, A. L. Chuvilin and V. L. Kuznetsov, *J. Vac. Sci. Technol. B*, 2000, **18**, 1059.
88 D. Xu, G. Guo, L. Gui, Y. Tang, Z. Shi, Z. Jin, Z. Gu, W. Liu, X. Li and G. Zhang, *Appl. Phys. Lett.*, 1999, **75**, 481.
89 O. R. Monteiro, V. P. Mammana, M. C. Salvadori, J. W. Ager III and S. Dimitrijevic, *Appl. Phys. A*, 2000, **71**, 121.
90 J.-M. Bonard, J.-P. Salvetat, Th. Stöckli, A. de Heer Walt, L. Forró and A. Châtelain, *Appl. Phys. Lett.*, 1998, **73**, 918.